Title

Etoposide-loaded immunoliposomes as active targeting agents for GD2-positive malignancies

Journal

Cancer Biology & Therapy, 15(7)

ISSN

1538-4047

Authors

Brown, Brandon S
Patanam, Tariq
Mobli, Keyan
et al.

Publication Date

2014-07-01

DOI

10.4161/cbt.28875

Peer reviewed

RESEARCH PAPER

Cancer Biology & Therapy 15:7, 851–861; July 2014; © 2014 Landes Bioscience

Etoposide-loaded immunoliposomes as active targeting agents for GD2-positive malignancies

Brandon S Brown[1,2], Tariq Patanam[2], Keyan Mobli[1,2], Christian Celia[2,3], Peter E Zage[4,5], Andrew J Bean[1,6,*], and Ennio Tasciotti[2]

[1]Department of Neurobiology and Anatomy and Graduate School of Biomedical Sciences; The University of Texas Health Science Center at Houston; Houston, TX USA; [2]Department of Nanomedicine; The Methodist Hospital Research Institute; Houston, TX USA; [3]Department of Pharmacy; University "G. d'Annunzio" of Chieti; Pescara, Chieti, Italy; [4]Dan L. Duncan Cancer Center; Baylor College of Medicine; Houston, TX USA; [5]Section of Hematology-Oncology; Department of Pediatrics; Texas Children's Cancer Center; Baylor College of Medicine; Houston, TX USA; [6]Division of Pediatrics; The University of Texas M.D. Anderson Cancer Center; Houston, TX USA

Keywords: immunoliposome, GD2, etoposide, neuroblastoma, drug delivery, nanomedicine, 3F8

Systemic chemotherapeutics remain the standard of care for most malignancies even though they frequently suffer from narrow therapeutic index, poor serum solubility, and off-target effects. In this study, we have encapsulated etoposide, a topoisomerase inhibitor effective against a wide range of cancers, in surface-modified liposomes decorated with anti-GD2 antibodies. We characterized the properties of the liposomes using a variety of methods including dynamic light scattering, electron microscopy, and Fourier transformed infrared spectroscopy. We examined whether these immunoliposomes were able to target cell lines expressing varying levels of surface GD2 and affect cellular proliferation. Anti-GD2 liposomes were generally targeted in a manner that correlated with GD2 expression and inhibited proliferation in cell lines to which they were efficiently targeted. The mechanism by which the immunoliposomes entered targeted cells appeared to be via clathrin-dependent uptake as demonstrated using flow cytometry and confocal microscopy. These studies suggest that anti-GD2-targeted, etoposide-loaded liposomes represent a potential strategy for more effective delivery of anti-cancer drugs that could be used for GD2 positive tumors.

Introduction

Systemic administration of chemotherapeutic drugs is the foundation of a majority of cancer treatment regimens ranging from neoadjuvant therapy to combination modality therapy.[1] Advancements in drug design and therapeutic strategies for adolescent malignancies have increased the overall 5-y survival to nearly 80%.[2] However, cytotoxic chemotherapeutics often suffer from a narrow therapeutic window and poor bioavailability. Accumulation of cytotoxic drugs can result in short and long-term off-target effects commonly in filtering organs such as the kidneys and liver. In this regard, approximately two thirds of patients suffer from at least one chronic health condition secondary to chemotherapy.[3]

Topoisomerase inhibitors (e.g., etoposide) are primary chemotherapeutics useful in the treatment of many forms of cancer. Etoposide is a topoisomerase II inhibitor that prevents re-ligation of unwinding DNA strands during DNA duplication causing double strand breaks, resulting in apoptotic cell death.[4] Pharmacokinetic studies of etoposide have suggested significant inter-individual variability in volume of distribution and systemic clearance rates in children with cancer.[5,6] Major side effects of etoposide include myelosuppression and acute hypotension due to activity of the drug on the bone marrow and cardiovascular system. Additionally, etoposide has been found to induce secondary leukemia in susceptible individuals due to off-site effects on hematopoietic stem cells.[7] Nephrotoxicity due to combination therapy with platinum-based drugs can influence blood levels of etoposide due to predominant clearance via the renal system.[8,9] Aside from pharmacokinetics, etoposide is poorly soluble in aqueous solutions necessitating slow infusion over 30–60 min and requires solubilizing agents such as surfactants and alcohols.[10]

The encapsulation of poorly soluble drugs in nanoparticles can enhance the therapeutic index and pharmacokinetics of cytotoxic treatments.[11] These nanotherapeutics are made from organic or inorganic materials, typically 10–200 nm in diameter, and can be produced in a variety of formulations and configurations that improve the delivery or protection of the therapeutic agents.[12-14] Lipid vesicles, particularly liposomes, possess the physiochemical features necessary for the encapsulation of hydrophobic and hydrophilic payloads into their lipid bilayer and aqueous compartments, respectively.[15,16] Liposomes coated with various hydrophilic agents can reduce reticuloendothelial uptake and prolong circulation time. For example, polyethylene glycol (PEG)-coated liposomes carrying the chemotherapeutic doxorubicin are currently used in clinical practice for diseases such as recurrent ovarian cancer and display decreased cardiotoxicity and increased circulatory half-life compared with native drug.[17,18] Etoposide has enhanced circulation kinetics and increased serum stability when stabilized into liposomes and lipid nanoparticles for both oral and intravenous delivery.[19-21]

*Correspondence to: Andrew J Bean; Email: a.bean@uth.tmc.edu
Submitted: 02/02/2014; Revised: 04/08/2014; Accepted: 04/13/2014; Published Online: 04/22/2014
http://dx.doi.org/10.4161/cbt.28875

Table 1. Liposome characteristics and drug loading as determined by dynamic light scatting and HPLC

	Size (± SD)	PDI	ZP (mV)	DL (%)	EE (%)
Blank liposomes	119.4 nm (2.4)	0.107	1.61 (0.1)	N/A	N/A
Etoposide liposomes	119.7 nm (1.4)	0.111	2.4 (0.8)	32.2	89.4
3F8 liposomes	129.4 nm (0.4)	0.105	–45.4 (4.6)	N/A	N/A
3F8 etoposide liposomes	128.1 nm (1.6)	0.116	–50.2 (1.9)	30.4	88.2

Four liposome formulations were characterized for size, polydispersity (PDI) and zeta potential (ZP) using dynamic light scattering. Drug-loading (DL) and encapsulation efficiency (EE) of etoposide within liposomes was then determined by HPLC analysis.

To improve the biodistribution of encapsulated agents, nanoparticles can be modified with targeting moieties that selectively bind to specific ligands preferentially expressed on the surface of the cancer cell. Surface functionalization of liposomes with targeting antibodies can be achieved by crosslinking targeting antibodies to either the lipids or the terminal ends of PEG chains extending from the outer liposomal membrane.[22] The use of PEG not only provides enhanced circulation time but also decreases the proximity of adjacent antibody molecules on the surface of the liposome therefore decreasing steric hindrance during targeting, and facilitating binding of the liposome to targets.[23,24] Cellular markers potentially targeted are specialized lipids like gangliosides.

Gangliosides are sialic acid-carrying glycosphingolipids expressed on all vertebrate tissues.[25] GD2 is a disialated ganglioside expressed on tumors of neuroendocrine origin such as melanoma, osteosarcoma, and neuroblastoma with natural expression constrained to peripheral and central nervous system tissues.[26,27] Previous studies have suggested that GD2 is expressed uniformly in neuroblastoma;[28] although variable expression has been reported between, and even within, cell lines.[29] Scarce non-pathological expression makes GD2 a useful entity for targeted therapies.[26] Monoclonal antibodies with specificity toward GD2 such as the 3F8 antibody displayed anti-tumor effects via antibody-directed cellular cytotoxicity as well as complement mediated cytotoxicity.[30-32] Although, additional immunomodulators like granulocyte macrophage colony-stimulating factor and interleukins are typically required for efficacy in clinical trials.[33] Anti-GD2 antibodies have shown promise as targeting agents.[34,35] Allen et al. produced liposomes carrying small interfering RNAs (siRNA) that were targeted to GD2 expressing cells resulting in the knockdown of the anaplastic lymphoma kinase gene.[36] Additionally, fenretinide, as well as the chemotherapeutic, doxorubicin have both been delivered with relatively specific binding to melanoma and neuroblastoma cells via anti-GD2 liposomes.[26,35]

In this study, we encapsulated etoposide into liposomes functionalized with the anti-GD2 monoclonal antibody 3F8, proved their specific targeting to GD2 expressing cancer cells and demonstrated how this approach would decrease the amount of drug required for cell killing.

Results

Preparation and characterization of immunoliposomes

DPPC liposomes were self-assembled via a modified ethanol injection technique that allowed for the simultaneous formation of liposomes and passive drug loading without direct extrusion.[37] This process resulted in stable 119.7 nm (± 1.4) particles with a polydispersity of 0.116 and zeta potential of 2.4 mV (± 0.8). The post-insertion process which integrates DSPE-mPEG2000-Maleimide conjugation groups onto the limiting membrane of the liposomes had a minor effect on size and surface charge, moving to 128.1 nm; while affecting the zeta potential which shows a value of –50.2 mV (± 1.9) (**Table 1**). TEM analysis revealed a monodispersed population, and immunogold labeling confirmed the presence of 3F8 antibodies conjugated to the surface of the nanoparticle (**Fig. 1A–C**). FTIR was used to assess the amine bonds found in the antibody (NH 1602 cm^{-1}), as well as the DSPE-mPEG2000 linker (CH 2920–2852 cm^{-1}, and CO 1700 cm^{-1}); both peaks were present in the conjugation product after ultrafiltration to remove unconjugated linker (**Fig. 1F**). Multiple formulations were produced in pilot experiments with varied ratios of DPPC and cholesterol as well as drug-to-lipid ratio, to enhance the entrapment efficiency and drug loading that were maximized at 88.2% and 30.4%, respectively (**Table 1**).

GD2 variable expression

Disialated gangliosides are variably expressed on the surface of cell types originating from the neural crest. Osteosarcoma, melanoma and an array of neuroblastoma cancer cell lines were evaluated by flow cytometry for GD2 expression using the GD2-specific 3F8 monoclonal antibody in conjunction with fluorescent secondary antibodies (**Fig. 2**). Treatment with fluorescent secondary antibodies alone has been used as a control, and GD2 expression was displayed as fold increase in fluorescent intensity over control fluorescence (**Fig. 2**). The neuroblastoma cell lines

Figure 1 (See opposite page). Physiochemical characterization of liposomes. (**A**) Transmission electron micrograph with negative staining of immunoliposomes examined at low magnification (scale bar: 1 μm). (**B**) Anti-GD2 immunoliposomes were incubated with anti-mouse IgG gold antibodies, washed, and negative-stained to assess anti-GD2 antibody distribution (scale bar: 100 nm). (**C**) Control liposomes without targeting antibodies were stained similarly to (**B**) with anti-mouse IgG gold and no gold was visible after negative staining (scale bar: 100 nm). (**D**) An immunoliposome schematic underlines the relative locations of associated drug, polyethylene glycol chains and anti-GD2 targeting antibodies. Multiple lamella were observed in some liposomes via transmission electron microscopy. (**E**) Dynamic light scattering data displays the mean liposomal hydrodynamic diameter and associated polydispersity. (**F**) Fourier transformed infrared spectra of ultrafiltered anti-GD2 antibody (top), maleimide polyethylene glycol polymer crosslinker (middle), and conjugation product of the two (bottom) depicts specific spectral peaks of each of the immunoliposome components. Boxes represent peaks of characteristic bonds in each component or the conjugation product.

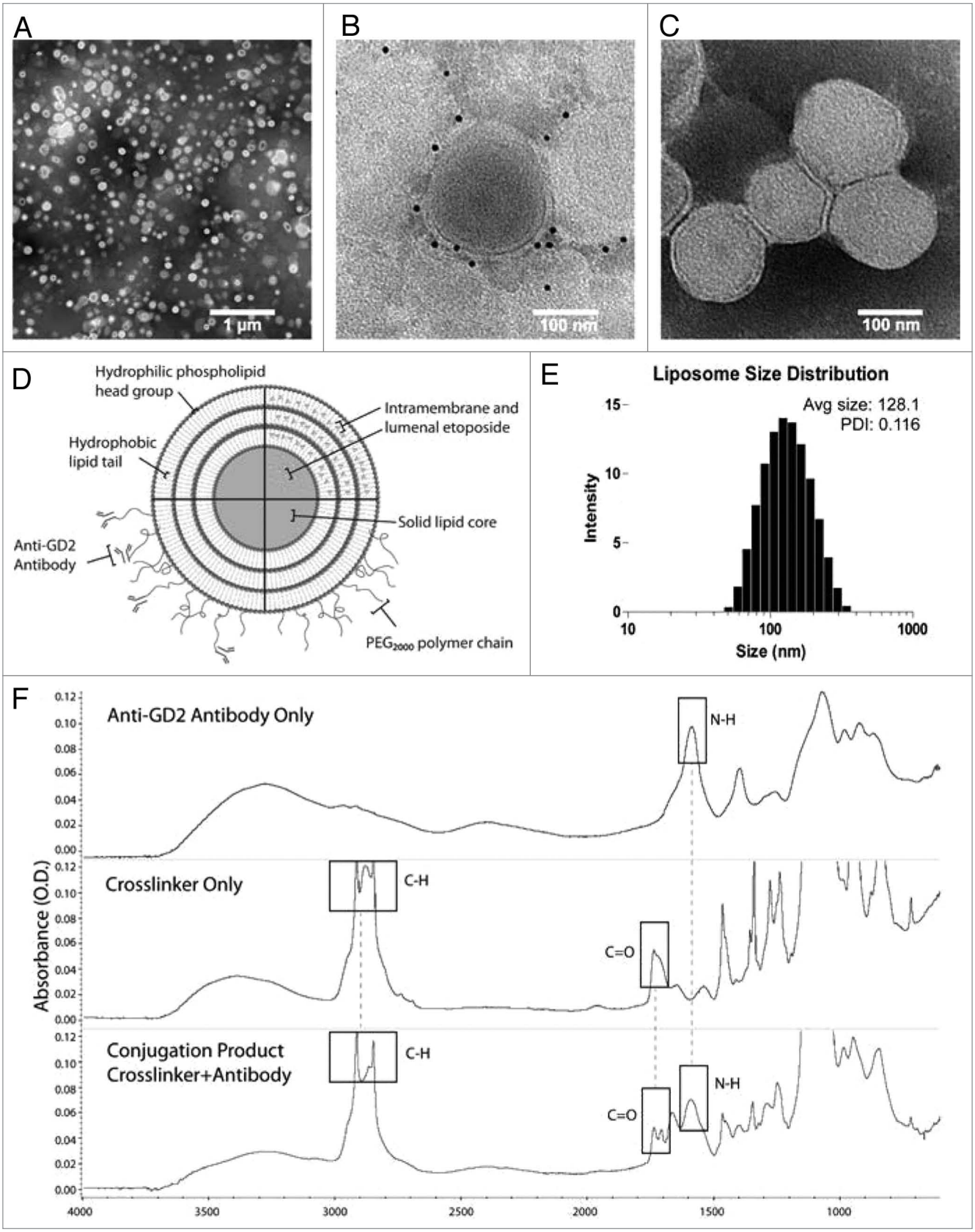

Figure 1. For figure legend, see page 852.

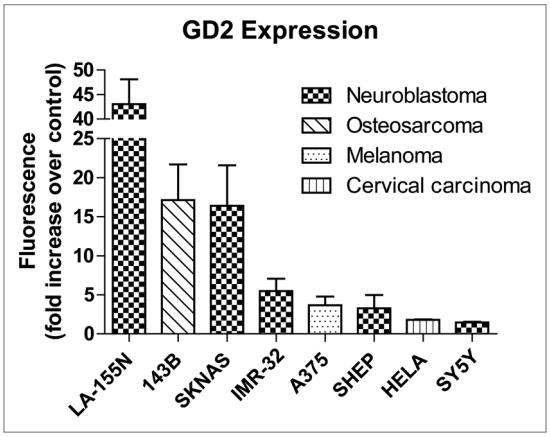

Figure 2. Surface GD2 expression. Eight cell lines from various cancer types were treated with anti-GD2 antibodies followed by fluorescent anti-mouse secondary antibodies or fluorescent secondary antibodies alone as a control and analyzed by flow cytometry. GD2 expression is represented by fold increases in geometric means of fluorescence intensity in anti-GD2 antibody + secondary antibody treated cells compared with cells incubated with secondary antibodies alone. Values represent averages of at least three independent experiments with at least 10 000 counts per experiment.

LA-155N and SKNAS as well as osteosarcoma 143B showed more than a 10-fold increase in GD2-associated fluorescence compared with control. Moderate GD2 expression was detected in IMR-32, SH-EP (both neuroblastoma), and A375 (melanoma) cell lines (**Fig. 2**). GD2-negative HeLa cervical carcinoma cells and SY5Y neuroblastoma cell lines each expressed little 3F8 reactivity suggesting low GD2 expression as previously described.[38] These data suggest that GD2 expression varies widely across tumor types and between different neuroblastoma cell lines.

Specific liposomal binding

The majority of anti-GD2 research focuses on GD2-positive or -negative cells, despite the potential clinical relevance of variable binding.[26,28,39] Quantitative assessment of targeting efficiency via flow cytometry revealed that GD2 expression was positively correlated with increased amounts of 3F8-mediated targeting in some, but not all cell lines. LA-155N and 143B both displayed a dramatic increase in targeting with liposomal labeling the entire population of cells analyzed by FACS (**Fig. 3A**, top). However, SKNAS cells that express high GD2 levels were only bound by 3F8 liposomes in 35% of analyzed cells, similar to that of moderate GD2 expressors (**Fig. 3A**, middle). Moderate GD2 expressors IMR-32, A375, and SH-EP were partially targeted by immunoliposomes with 22.1%, 30.7% and 35.9% positively labeled compared with control liposomes, respectively (**Fig. 3A**, bottom; **Fig. 4A**, top). Histogram plots showing fluorescence intensity of targeted vs. untargeted liposomes show the relative shift after targeted liposomal binding. Notably, only high GD2-expressors had complete intensity shifts following the treatment (**Figs. 3C and 4C**). As expected, GD2-negative cell lines HeLa and SY5Y were bound by 3F8 immunoliposomes at levels comparable to nonspecific anti-IgG liposomes (**Fig. 4A**, bottom). Negative controls, immunoliposomes targeted to the unrelated STAM cytoplasmic protein, or labeled with nonspecific IgG antibodies, displayed insignificant cell binding in all cell lines (**Figs. 3A and 4A**).

Immunoliposome uptake and endocytosis inhibition

To examine binding in physiologic conditions in vitro, SKNAS cells were seeded in chamber slides and treated with rhodamine-labeled liposomes at 37 °C for 30 min. Confocal analysis revealed that targeted immunoliposomes significantly accumulated on GD2 positive cells compared with untargeted liposomes (**Fig. 5A**). To further investigate particle internalization, dynasore and filipin were utilized to block clathrin or caveolin-dependent endocytosis respectively.[40] Average liposomal fluorescence after treatment with inhibitors and liposomes was quantified by drawing regions of interest around individual cells and calculating mean intensities across treatment groups. Dynasore inhibition restricted receptor mediated endocytosis of immunoliposomes via clathrin-coated pits while filipin inhibition of the caveolar pathway had no effect on liposomal uptake (**Fig. 5B and C**), in accordance with literature on immunoliposome uptake.[41]

In vitro inhibition of GD2 positive cell growth

We observed that anti-GD2 immunoliposome treatment was more cytotoxic compared with both untargeted liposomes and drug alone in GD2-positive cells (**Fig. 6A and B**). IC_{50} values of etoposide-loaded anti-GD2 immunoliposomes in GD2 positive cell lines LA-155N and 143B were 37.09 μg/mL and 66.16 μg/mL whereas the IC_{50} for the untargeted etoposide-loaded liposomes for LA-155N and 143B was 80.06 μg/mL and 111.9 μg/mL respectively. The GD2 negative cell line SY5Y had no significant improvement of IC_{50} in anti-GD2 immunoliposomes over untargeted liposomes, although liposomal etoposide encapsulation did increase toxicity at both 100 and 200 μg/mL compared with free drug (**Fig. 6C**). For these studies, two-way ANOVA was performed with a Bonferroni post-test to compare means of specific concentrations. Significance was defined as a P value < 0.05.

Discussion

We have designed, prepared, and physiochemically characterized etoposide-loaded anti-GD2 immunoliposomes. Ethanol-injection methods paired with post-insertion of 3F8 anti-GD2 antibodies produced liposomes with maximal drug loading and optimal antibody modification. These immunoliposomes targeted to an array of GD2-positive cell lines and inhibited tumor cell proliferation in vitro. These data suggest that encapsulating etoposide inside immunoliposomes may provide selective delivery of the chemotherapeutic, limit off target effects, enhance kinetics, and decrease systemic dosage.

Etoposide-liposomes displayed consistent size distribution and uniformity without using an extrusion technique. This procedure allowed for the simultaneous encapsulation of up to 4 mg/mL etoposide into 10 mM liposomal formulations with a surface charge of –50.2 mV, comparing favorably to other etoposide formulations.[19,20,42] The anionic surface charge was ideal because previous studies have indicated that cationic liposomes fuse with endothelial cell membranes nonspecifically, and neutrally charged liposomes tend to aggregate prior to and during

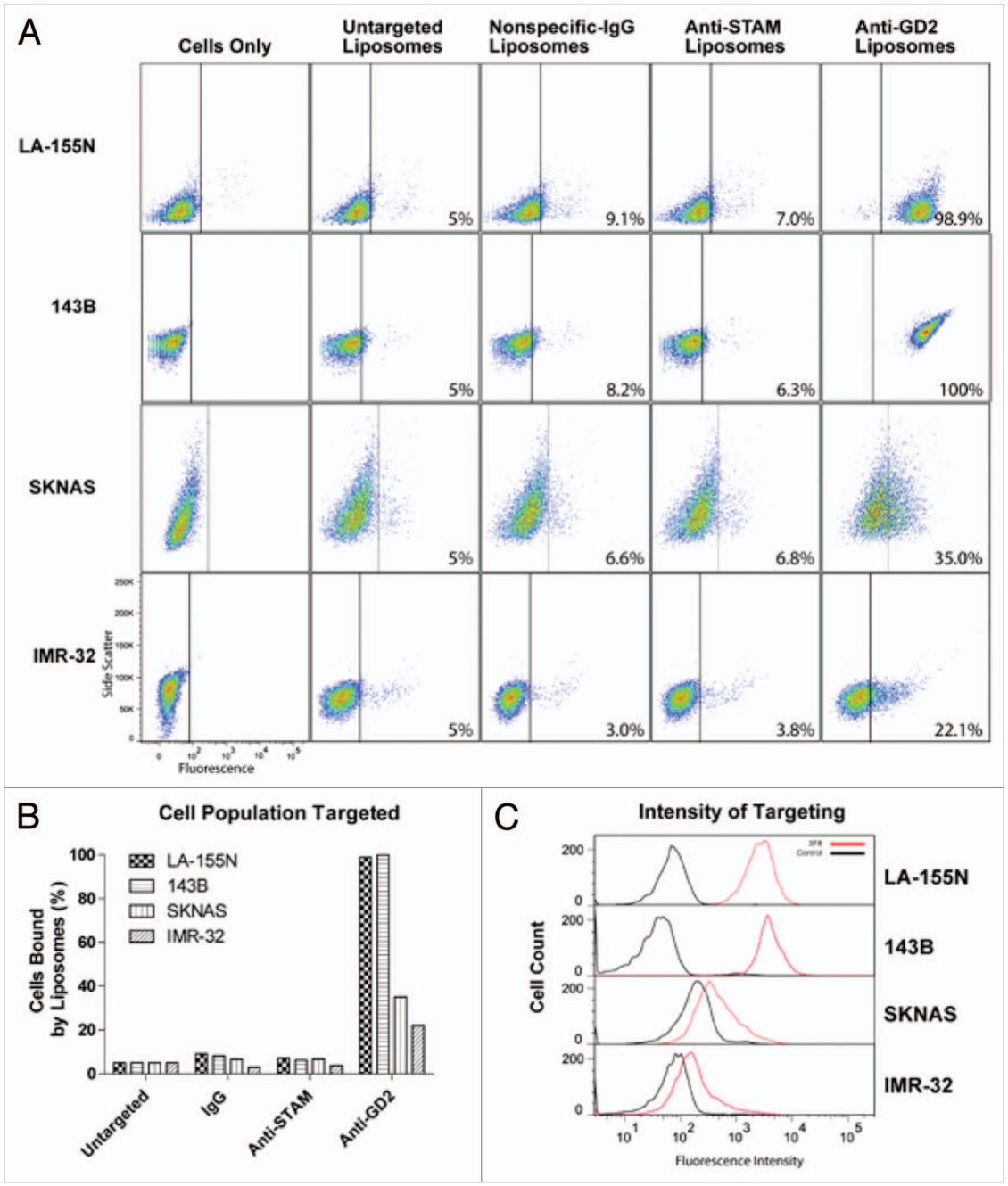

Figure 3. Liposome targeting in cells with high GD2 expression. Liposome and immunoliposome formulations produced with equivalent amounts of fluorescent lipids were incubated with LA-155N, 143b, SKNAS and IMR-32 cell lines for 30 min on ice. We evaluated the surface attachment of fluorescently labeled targeted vs untargeted or mistargeted liposomes to the surface of cells by flow cytometry. Fluorescence thresholds were set at the 95% fluorescence percentile for each cell line treated with fluorescent untargeted control liposomes. (**A**) Density plots are arranged by side scatter vs fluorescent intensity of cell lines (left) treated with one of the four liposome formulations (untargeted, nonspecific-IgG, anti-STAM, or anti-GD2) and analyzed by flow cytometry. (**B**) Cell populations with positive binding by liposomes are represented graphically as a percent of total cell populations recorded above the threshold. (**C**) Histograms represent fluorescent intensity of recorded cells treated with fluorescent untargeted liposomes (black) compared with fluorescent anti-GD2 immunoliposomes (red).

administration. Hence, the anionic immunoliposome charge resulted in a stable colloidal suspension prior to treatment followed by ligand specific binding without nonspecific cationic interactions between immunoliposomes and cell membranes.[43] Maintaining appropriate temperature and ethanol to PBS ratios was crucial in maintaining liposomal diameters below 125 nm. Liposomal size between 100 and 200 nm has been shown to reduce clearance from circulation compared with smaller and larger liposomes, that accumulate in the liver and spleen, respectively.[44,45]

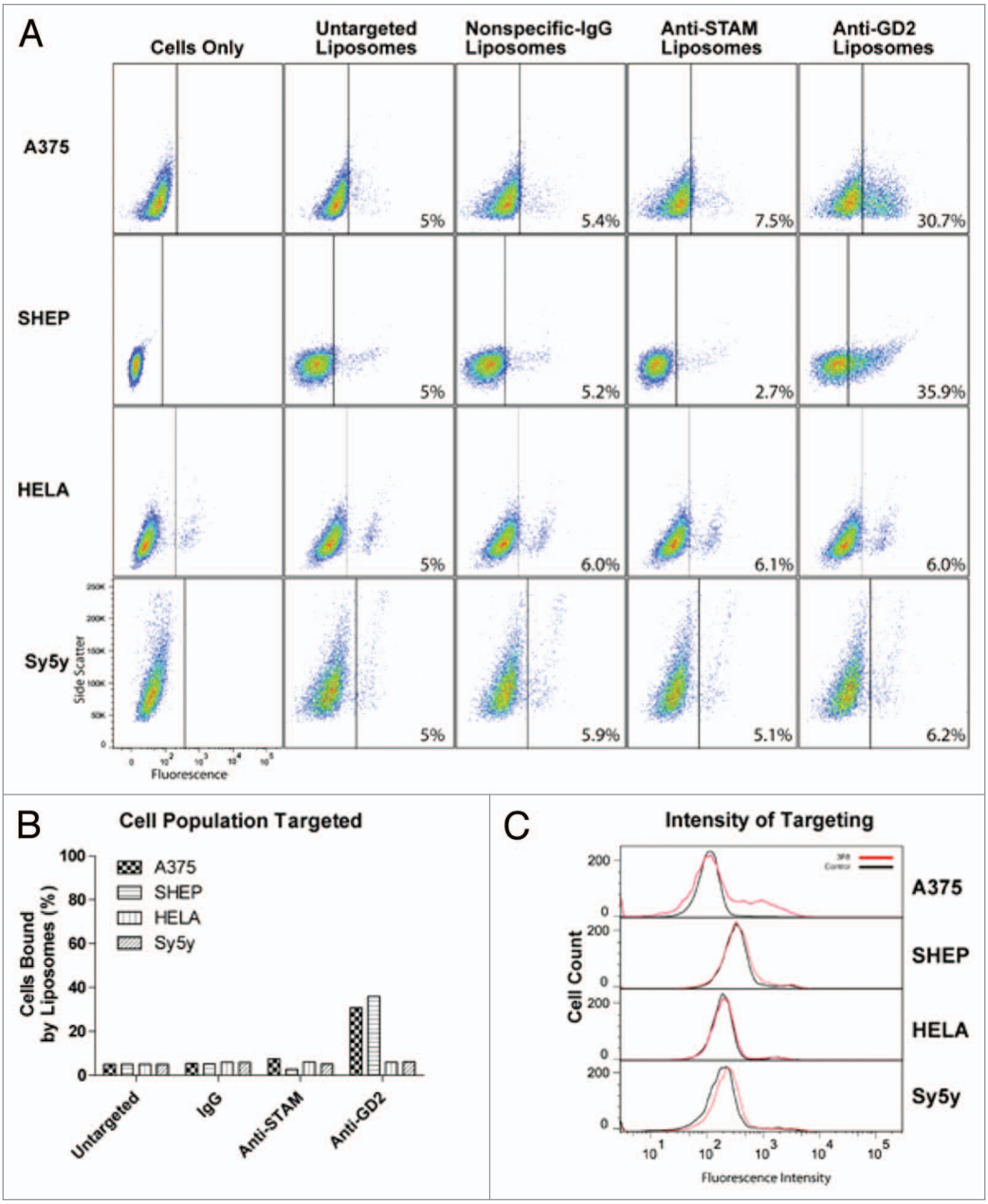

Figure 4. Liposome targeting in the four cell lines tested with the lowest GD2 expression. Liposome and immunoliposome formulations with equivalent amounts of fluorescent lipids were incubated with A375, SHEP, HELA, and SY5Y cell lines for 30 min on ice. We evaluated the surface attachment of fluorescently labeled targeted vs untargeted or mistargeted liposomes to the surface of cells by flow cytometry. Fluorescence thresholds were set at the 95% fluorescence percentile for each cell line treated with fluorescent untargeted control liposomes. (**A**) Density plots are arranged by side scatter vs fluorescent intensity of cell lines (left) treated with one of the four liposome formulations (untargeted, nonspecific-IgG, anti-STAM, or anti-GD2) and analyzed by flow cytometry. (**B**) Cell populations with positive binding by liposomes are represented graphically as a percent of total cell populations recorded above the threshold. (**C**) Histograms represent fluorescent intensity of recorded cells treated with fluorescent untargeted liposomes (black) compared with fluorescent anti-GD2 immunoliposomes (red).

Following liposome preparation, ethanol is positioned at higher concentrations at the lipid/water interface, thus increasing drug retention and entrapment efficiency in liposomes.[37] The slight partition of ethanol at the outer leaflet of the bilayer allows for simple removal by negative pressure evaporation before systemic administration, without affecting drug release kinetics.[46] Etoposide release from the immunoliposomes was observed at a stable rate from 6 to 72 h at physiologic temperature and pH.

GD2 expression is limited to tumors of neural crest origin and peripheral nerves.[47,48] Our studies suggest that anti-GD2 targeted liposomes accumulate on GD2-positive cell lines heterogeneously with respect to GD2 expression. We found variable expression of GD2 surface-expression among an array of tumor cell

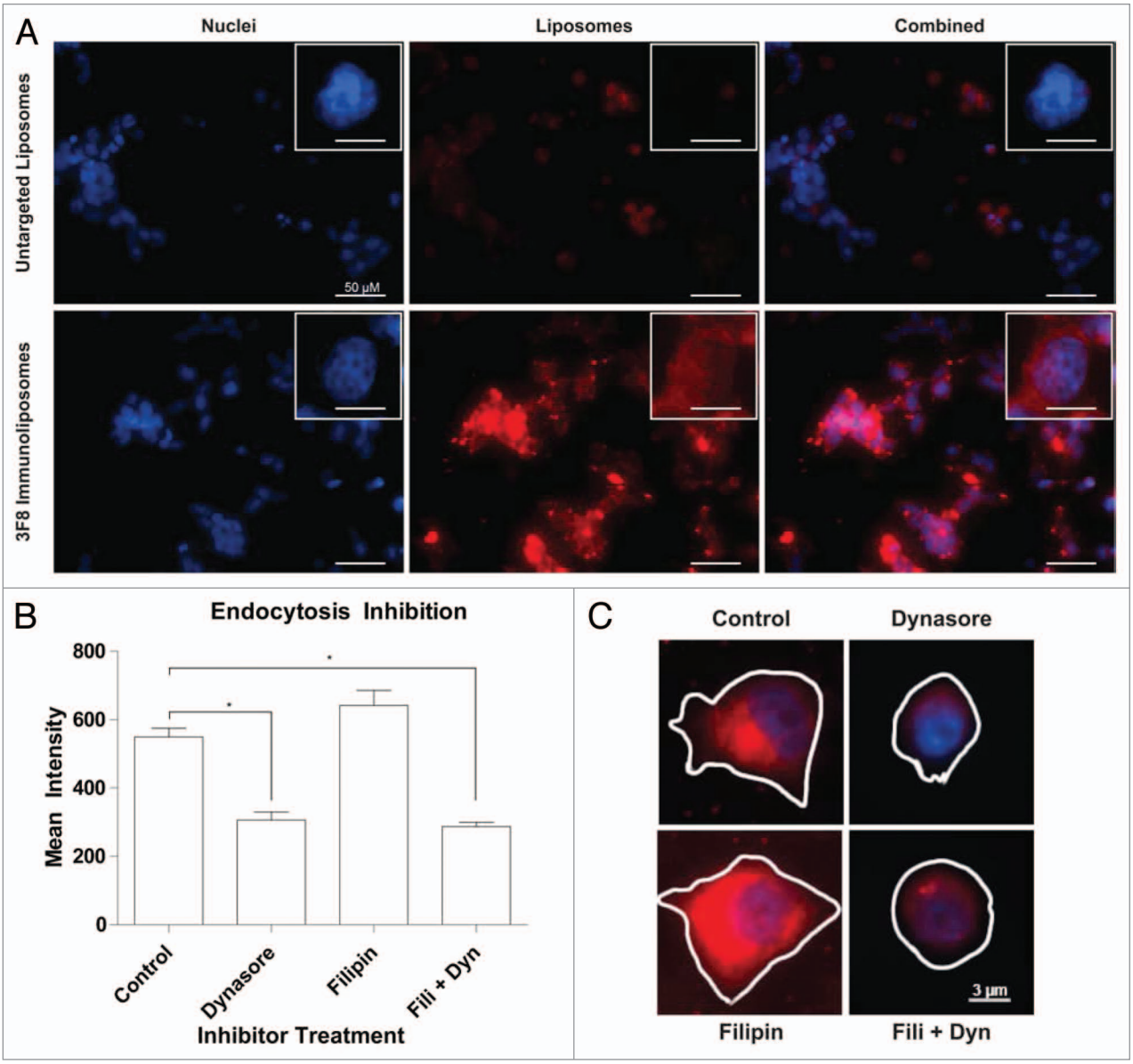

Figure 5. In vitro liposomal uptake. (**A**) LA-155N cells were incubated with liposomes at 37 °C for 30 min followed by confocal microscopy analysis. Uptake of untargeted or anti-GD2 targeted liposomes (red) was examined. Cells were also labeled with a nuclear DAPI stain (blue). (**B**) SKNAS cells were incubated with the endocytosis inhibitor Dynasore, Filipin, or both drugs for 30 min followed by co-incubation of inhibitors and fluorescent untargeted or anti-GD2 immunoliposomes for 1 h. Cells were washed, fixed, and imaged by fluorescence microscopy. Regions of interest were drawn around representative cell perimeters and cytosolic fluorescent intensities were recorded from at least 20 fields of view for each treatment group. Means were compared by one way ANOVA for significance. *$P < 0.05$. (**C**) Representative images from the fluorescent microscope of cells treated with Filipin, Dynasore, a combination of the two, or no drug in addition to anti-GD2 liposomes.

lines including neuroblastoma, melanoma, and osteosarcoma. Liposomal encapsulation of etoposide significantly decreases the antiproliferative IC_{50} for etoposide compared with unencapsulated drug in multiple cell lines. Moreover, 3F8 immunoliposomes inhibit cell proliferation more effectively in cell lines with higher GD2 expression suggesting that targeting etoposide could decrease the concentration of drug required for anti-proliferative effects. However, antiproliferative concentrations of anti-GD2 etoposide liposomes were comparable for two cell lines, LA-155N and 143B, with significantly different GD2 expression. Lack of differential effects on proliferation between tumor lines may be due to different endocytic behavior across tumor types or a ceiling effect on the ability of cells to internalize liposomes. We have observed a correlation between cellular GD2 levels and the ability to target cells using etoposide-containing, GD2-targeted liposomes. Strong anti-GD2 targeting in cell lines that express high levels of GD2 is consistent with previous studies.[26,35,49] Free 3F8 antibodies were used initially in pilot experiments but were discontinued due to the lack of independent cytotoxicity observed. Antiproliferative effects of free 3F8 antibodies are expected in

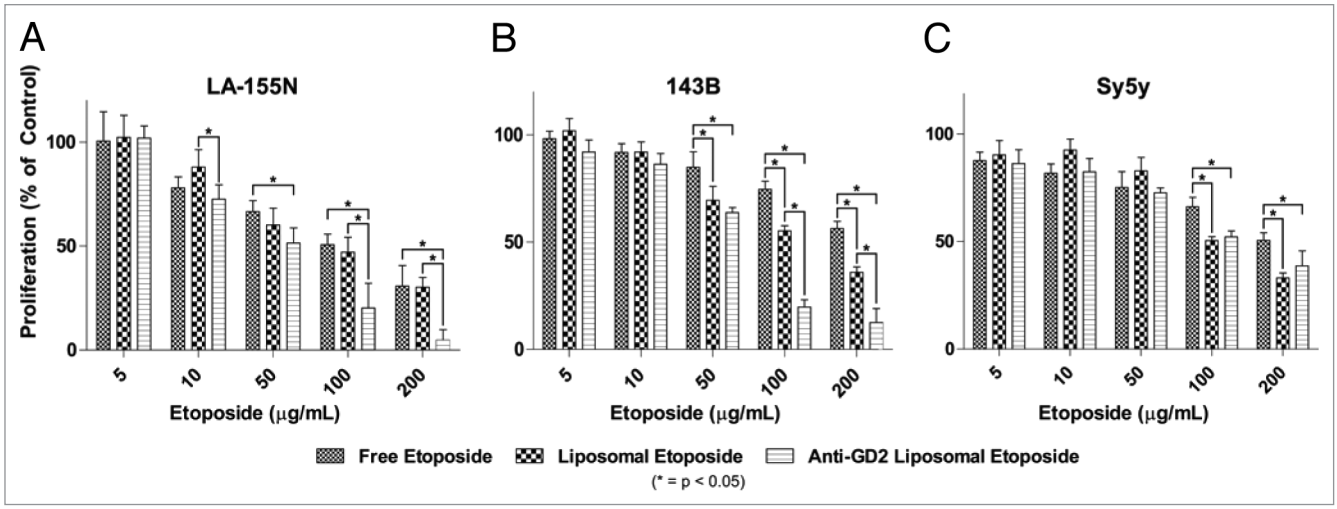

Figure 6. Inhibition of cell proliferation in vitro. Tumor cells were seeded in 96-well plates and treated with various concentrations of free etoposide, liposomal etoposide, or anti-GD2 immunoliposomal etoposide for 24 h followed by an MTT viability assay. (**A and B**) High GD2 expressing neuroblastoma (LA-155N) and osteosarcoma (143B) cell lines were evaluated for proliferation after etoposide treatment. (**C**) Low GD2 expressing neuroblastoma cells (SY5Y) were also tested for changes in proliferation at etoposide concentrations 5–200 μg/mL. Mean viabilities were compared by two-way ANOVA with Bonferroni posttests between treatment types for significance. *$P < 0.05$.

vivo with the presence of complement proteins and circulating leukocytes not present in our in vitro studies.[30,50]

Inhibition of endocytosis following dynasore and filipin treatment suggests that clathrin plays a role in the internalization of anti-GD2 immunoliposomes. Inhibition of cell proliferation after treatment with etoposide-loaded particles suggests that the delivery of etoposide via liposomes can provide therapeutic benefit to slow the growth of tumors. Decreased cancer cell growth following drug-loaded immunoliposome treatment suggests that etoposide escapes the liposome and the cellular endolysosomal compartment and reaches the nuclear compartment where it is able to inhibit topoisomerase II activity. The mechanism by which encapsulated etoposide escapes lysosomal degradation remains unclear. One possibility is that lipophilic etoposide is transferred to the plasma- and endocytic-membranes during liposome interaction with target cells, as observed for other lipophilic drugs delivered by immunoliposomes.[22] Additional etoposide may reach tumor cells when liposomes degrade in the extracellular space within the tumor microenvironment.[20]

In conclusion, liposomes targeted with anti-GD2 antibodies were synthesized using an ethanol injection method resulting in high etoposide encapsulation. Targeted liposomes accumulated on GD2 expressing cell lines. The targeting of immunoliposomes and the expression of GD2 on cell lines was highly correlated in cells with high GD2 expression. We observed that the encapsulation of etoposide in 3F8-decorated liposomes significantly inhibited cellular proliferation in GD2 expressing LA-155N and 143B cells. Clathrin-dependent uptake was identified as a mechanism by which the liposomes gained entry into cells, although the mechanism by which the etoposide escapes from the internalized liposome and endolysosomal compartments to affect cellular proliferation remains unclear. These data collectively suggest that the GD2 immunoliposome formulation could increase therapeutic effect of etoposide, warranting in vivo targeting and safety evaluation.

Materials and Methods

Chemicals and lipids

Dipalmitoyl-sn-glycero-3phosphochiline (DPPC), 1,2-dioleoyl-sn-glycero-3-phosphoethanolamine-N-(lissamine rhodamine B sulfonyl) (DOPE-Rhodamine), 1,2-distearoyl-*sn*-glycero-3-phosphoethanolamine-N-[methoxy(polyethylene glycol)-2000] (DSPE-mPEG2000) and 1,2-distearoyl-*sn*-glycero-3-phosphoethanolamine-N-[maleimide(polyethylene glycol)-2000] (DSPE-mPEG200-Maleimide) were purchased from Avanti Polar Lipids. 3β-hydroxy-5-cholestene (cholesterol), >99% dimethyl sulphoxide (DMSO), thiazolyl blue tetrazolium bromide (MTT salt), L-glutamine, tris-HCl, 40% Glycerol, red ponceau, and Tris buffered saline (TBS) were obtained from Sigma Aldrich. Traut's reagent, penicillin, streptomycin, bromophenol blue, and all cell culture media were acquired from ThermoFisher Scientific. Etoposide (VP16, >99% grade purity) was obtained from Biotang. Tween 20 was acquired from Aurion. Horseradish peroxidase was purchased from Cell Signaling Technology. Alexa Fluor 488 goat anti-mouse IgG was purchased from Invitrogen. Murine IgG3 monoclonal antibody 3F8 (3F8 anti-GD2) was a kind gift from Nai-Kong Cheung (Memorial Sloan Kettering Cancer Center). All other chemicals were of analytical grade and purchased from Sigma Aldrich.

Liposome preparation and physicochemical characterization

Liposomes were prepared using a modified ethanol direct injection technique previously reported.[46] Briefly, DPPC and cholesterol at a molar ratio of 60:40 were dissolved in 100% ethanol heated to 60 °C under continuous stirring. Then, 0.2 mol% of the fluorescent lipid, DOPE-Rhodamine was dissolved into

ethanol and injected into a warm solution of PBS at a ratio of 1:9 by volume under continuous stirring (2000 rpm). The ethanol was then removed by rotary evaporation (Buchi). Where necessary, etoposide dissolved in DMSO (at 50 mg/mL) was added to the ethanol phase prior to injection, thus obtaining a final concentration in the range from 1 to 4 mg/mL. Entrapment efficiency and drug loading were calculated by the following formulas:

Entrapment Efficiency (%) = (Quantity of drug encapsulated) / (Total quantity of drug added) × 100%

Drug Loading (%) = (Quantity of drug encapsulated) / (Total quantity of lipids added) × 100%

Average size, size distribution, and zeta potential were analyzed using Malvern Zetasizer Nano ZS (Malvern) as previously reported.[51] Briefly, liposomes were diluted (1:100 molar ratio) using isotonic PB buffer (pH 7.4), previously filtered (pore size 0.22 mm) through polypropylene membranes (Whatman Inc.) to avoid multiscattering phenomena and loaded into size and Z-potential disposable cuvettes before analysis. Photocorrelation spectroscopy was applied to evaluate average size and narrow size distribution. The instrument was set up using the following parameters: real refractive index 1.59, imaginary refractive index 0.0, medium refractive index 1.330, medium viscosity 1.0 mPa × s and medium dielectric constant 80.4. Z-potential was performed using the Doppler laser anemometry and hence the electrophoretic mobility. A Smoluchowsky constant F (Ka) of 1.5 was applied to measure electrophoretic mobility of samples.

Preparation of 3F8 anti-GD2 immunoliposomes

Micelles containing DSPE-mPEG2000 and DSPE-mPEG2000-maleimide at a 99:1 molar ratio were co-dissolved in an ethanol solution and added drop wise into a warm PBS solution containing 2 mM EDTA at a ratio of 1:1 v/v creating the final micellar solution. Fifty microliters of micellar solution (10 mM, pH 7.4) was added to the preformed liposome mixture with agitation and heating at 65 °C thus allowing post insertion. Meanwhile, 3F8 anti-GD2 monoclonal antibodies were sulfonated at a 1:10 molar ratio using Traut's reagent and purified using Zebaspin desalting columns (ThermoFisher Scientific). After the liposomal solution returned to room temperature, the purified sulfonated antibody was added to the liposomal solution and incubated at 4 °C overnight under constant stirring to obtain the final immunoliposomes.

Transmission electron microscopy (TEM)

TEM analysis was performed using a JEM 1010 transmission electron microscope (JEOL, Inc.) at a voltage of 80 kV. Liposomes underwent negative staining and placed on formvar coated carbon grids followed by 1 min staining with 1% v/v ammonium molybdate (pH 7.0). Immunogold staining of samples was performed by blocking liposomes for 30 min with 5% BSA in PBS solution (pH 7.4), followed by 30 min incubation with secondary goat-anti-mouse IgG 6 nm gold antibodies (1:25 v/v dilution) followed by three washes in water to remove salts and unbound immunogold IgG.

Fourier transformed infrared spectroscopy (FTIR)

Bonds conjugated with DSPE-mPEG2000-Maleimide linker and the 3F8 antibody were qualitatively identified by using the FTIR apparatus. Concentrated samples (10 mM) were prepared by the application of 3 μL followed by desiccation on the SMART ATR diamond surface on a Nicolet 6600 FTIR spectrophotometer. The DSPE-mPEG2000-Maelimide and 3F8 antibody were analyzed individually and then conjugated. Unconjugated linker was removed by Zebaspin desalting columns followed by Amicon centrifuge filters (Millipore) with a 30 kDa molecular weight cutoff at 14 000 × g for 10 min prior to analysis of the conjugated sample. The detector was used at room temperature at a 4 cm^{-1} resolution in absorbance mode averaging 16 runs. Peak analysis was performed using Omnic Spectra software.

Cell culture

Neuroblastoma cell lines NBLS, LA-155N, IMR-32, SH-EP, and SH-SY5Y were validated by STR analysis and cultured in DMEM/F12. Cervical carcinoma HeLa and breast carcinoma MDA-MB-231 cell lines were cultured in DMEM and Leibovitz L15 respectively. Malignant melanoma cell lines SK-MEL-28 and A375 were cultured in DMEM. Osteosarcoma cell line 143B was also cultured in DMEM. All media was supplied with FBS (10% v/v), penicillin G-streptomyocin mixture (1% v/v), and L-glutamine (1% v/v). Cell lines were cultured in incubators at 37 °C and 5% CO_2.

FACS analysis of GD2 expression and liposome targeting

In order to assess the expression of GD2 on the surface of different cell lines, 3×10^5 cells per treatment group of each line were collected. Cells were mobilized using a 2 mM treatment of EDTA to retain surface protein structure and counted using hemocytometry. They were then re-suspended in 3% v/v BSA in PBS solution (pH 7.4) and placed on ice for the remainder of the analysis. After 30 min of blocking in 3% v/v BSA, cells were treated with primary 3F8 antibodies and incubated for 1 h. Cells were then washed in BSA solution and further incubated for 30 min with Alexa Fluor 488 goat anti-mouse IgG. Control groups were treated with secondary antibody only. After final washing in PBS solution (pH 7.4), samples were analyzed by the Fortessa cell counter (Becton Dickinson) with excitation at 488 nm and an emission bandpass filter at 530 nm.

Liposome targeting to cancer cells

To assess 3F8 immunoliposome targeting to the cell lines mentioned, 3×10^5 cells of each line were collected and counted as herein reported. The collected cells were exposed to DOPE-Rhodamine liposomes with or without targeting agents for 30 min under continuous rotation (10 rpm) at 4 °C. Each treatment group was washed three times with PBS solution (pH 7.4) and analyzed on the FACS Fortessa cell counter (Becton Dickinson) with excitation at 488 nm and an emission bandpass filter at 530 nm.

Confocal imaging of liposome uptake

Optical analysis of liposome uptake was done on the Nikon A1 confocal laser scanning microscope (Nikon Corporation). Cells were grown on 4-well chamber slides at a seeding density of 7×10^4 cells per well and allowed to attach overnight. Cells were treated with 3F8 immunoliposomes or untargeted liposomes for 30 min in cell culture conditions. Prior to imaging, cells were fixed with 4% v/v paraformaldehyde and mounted with Prolong Gold with DAPI.

H.P.L.C. quantification of drug loading

The amount of etoposide entrapped inside liposomes was performed using high performance liquid chromatography (H.P.L.C.) (Hitachi). Etoposide loaded liposomes were separated from unencapsulated etoposide by ultracentrifugation at 150 000 × g at 4 °C for 1 h in a Fiberlite F50L-24 × 1.5 rotor, followed by Amicon filtration with 30 kDa centrifuge filters at 14 000 × g for 10 min. Filtered liposomes were then diluted in methanol followed by injection and flow through a Zobrax Eclipse Plus C18 column (4.6 mm × 150 mm, i.d. 5 μm) (Agilent Technologies) at a flow rate of 0.65 mL/min. The mobile phase was composed of 50% v/v methanol and 50% v/v acetic acid. Absorbance was detected at 228 nm, and samples were run in triplicate. Results are the average of three different measurements ± standard deviation.

In vitro proliferation study

Neuroblastoma cells (cell line: LA-155N, or SY5Y) and osteosarcoma cells (cell line: 143B) were seeded at a cell density of 7500 cells/well using 96 well cell culture plates. Cells were allowed to attach overnight in the incubator after which the media was removed and replaced with treatment solutions. Cells were treated with 100 μL PBS, etoposide alone (control), untargeted etoposide liposomes, or 3F8 targeted etoposide loaded liposomes at etoposide concentrations increasing from 0 to 200 μg/mL. Viability studies were performed via MTT assay (Sigma Aldrich). MTT reduction at time 24 h was assessed by absorbance measurement at 570 nm with a reference wavelength of 690 nm according to the manufacturer's instructions. IC_{50} calculations were performed via nonlinear regression via GraphPad Prism software v5.03.

Endocytosis inhibition study

To assess through which pathway immunoliposomes were internalized, SKNAS neuroblastoma cells were cultured on chamber slides as described previously. The cells were washed twice with PBS and the media was replaced with culture medium without serum to avoid serum inactivation of inhibitors. The cells were pretreated Dynasore (80 μM), Filipin (10 μM), or a combination of both drugs for 30 min. Rhodamine-labeled 3F8 immunoliposomes (0.1 mM) were then added for 1 h at 37 °C to allow for internalization. Cells were washed three times with PBS, fixed with 4% v/v paraformaldehyde and mounted with DAPI Prolong Gold antifade reagent (Molecular Probes). Cells without inhibitors treated with and without immunoliposomes served as positive and negative controls, and cells were treated with fluorescent EGF to verify inhibition of clathrin-dependent endocytosis. Twenty fields of view were captured and analyzed for mean fluorescent intensity of Rhodamine within individual cells delineated by regions of interest on Nikon Elements software version 3.22. Intensity means were compared by one way ANOVA, and P values < 0.05 were considered significant.

Etoposide release study

Differences in drug release between liposomes and immunoliposomes were realized in a 72 h release study. Particles were centrifuged in a 3.5 mL Amicon Ultra-4 100 kDa filter at 4000 × g for 30 min and resulting supernatant was diluted to reach 3.5 mL volume. One milliliter of colloidal particles was placed in Spectra/Por Float-A-Lyzer G_2 cellulose ester membranes (MWCO 100kD, 1mL vol) for 72 h with samples collected at different time points. The receptive phase consisted of a 50 mL solution of PBS (pH 7.4) and Tween20 (1% v/v). Study was conducted at 37 °C under continuous stirring (300rpm) and 1mL samples withdrawn were replaced with new PBS + Tween20 solutions. Samples were analyzed via HPLC as previously reported.

Disclosure of Potential Conflict of Interest

The authors have no conflicts of interest to disclose.

Acknowledgments

These studies were funded in part by NIH grant (CA166749), Innovator Extension Grant (W81XWH-12-1-0414), and R21 (R21CA173579). The authors would like to thank Dr Ananth Anapragada, Dr M Waleed Gaber, Kenn Dunnar Jr., Natalie Sirisaengtaksin, Monica Gireud, Denisse Meza, Dr Alessandro Parodi, D Haviland, and The Methodist Hospital Research Institute Flow Cytometry Core Facility.

References

1. Siegel R, DeSantis C, Virgo K, Stein K, Mariotto A, Smith T, Cooper D, Gansler T, Lerro C, Fedewa S, et al. Cancer treatment and survivorship statistics, 2012. CA Cancer J Clin 2012; 62:220-41; PMID:22700443; http://dx.doi.org/10.3322/caac.21149
2. Bhatia S. Long-term complications of therapeutic exposures in childhood: lessons learned from childhood cancer survivors. Pediatrics 2012; 130:1141-3; PMID:23166341; http://dx.doi.org/10.1542/peds.2012-2884
3. Oeffinger KC, Mertens AC, Sklar CA, Kawashima T, Hudson MM, Meadows AT, Friedman DL, Marina N, Hobbie W, Kadan-Lottick NS, et al.; Childhood Cancer Survivor Study. Chronic health conditions in adult survivors of childhood cancer. N Engl J Med 2006; 355:1572-82; PMID:17035650; http://dx.doi.org/10.1056/NEJMsa060185
4. Montecucco A, Biamonti G. Cellular response to etoposide treatment. Cancer Lett 2007; 252:9-18; PMID:17166655; http://dx.doi.org/10.1016/j.canlet.2006.11.005
5. Evans WE, Sinkule JA, Crom WR, Dow L, Look AT, Rivera G. Pharmacokinetics of Teniposide (VM26) and etoposide (VP16-213) in children with cancer. Cancer Chemother Pharmacol 1982; 7:147-50; PMID:7083455; http://dx.doi.org/10.1007/BF00254537
6. Lowis SP, Pearson AD, Newell DR, Cole M. Etoposide pharmacokinetics in children: the development and prospective validation of a dosing equation. Cancer Res 1993; 53:4881-9; PMID:8402676
7. Ezoe S. Secondary leukemia associated with the anticancer agent, etoposide, a topoisomerase II inhibitor. Int J Environ Res Public Health 2012; 9:2444-53; PMID:22851953; http://dx.doi.org/10.3390/ijerph9072444
8. McLeod HL, Evans WE. Clinical pharmacokinetics and pharmacodynamics of epipodophyllotoxins. Cancer Surv 1993; 17:253-68; PMID:8137343
9. Rodman JH, Murry DJ, Madden T, Santana VM. Altered etoposide pharmacokinetics and time to engraftment in pediatric patients undergoing autologous bone marrow transplantation. J Clin Oncol 1994; 12:2390-7; PMID:7964955
10. Joel SP, Shah R, Slevin ML. Etoposide dosage and pharmacodynamics. Cancer Chemother Pharmacol 1994; 34(Suppl):S69-75; PMID:8070031; http://dx.doi.org/10.1007/BF00684867
11. Bertrand N, Wu J, Xu X, Kamaly N, Farokhzad OC. Cancer nanotechnology: The impact of passive and active targeting in the era of modern cancer biology. Adv Drug Deliv Rev 2014; 66C:2-25; PMID:24270007; http://dx.doi.org/10.1016/j.addr.2013.11.009
12. Godin B, Tasciotti E, Liu X, Serda RE, Ferrari M. Multistage nanovectors: from concept to novel imaging contrast agents and therapeutics. Acc Chem Res 2011; 44:979-89; PMID:21902173; http://dx.doi.org/10.1021/ar200077p
13. Paolino D, Licciardi M, Celia C, Giammona G, Fresta M, Cavallaro G. Folate-targeted supramolecular vesicular aggregates as a new frontier for effective anticancer treatment in in vivo model. Eur J Pharm Biopharm 2012; 82:94-102; PMID:22705641; http://dx.doi.org/10.1016/j.ejpb.2012.06.001
14. Sanhai WR, Sakamoto JH, Canady R, Ferrari M. Seven challenges for nanomedicine. Nat Nanotechnol 2008; 3:242-4; PMID:18654511; http://dx.doi.org/10.1038/nnano.2008.114

15. Al-Jamal WT, Kostarelos K. Liposomes: from a clinically established drug delivery system to a nanoparticle platform for theranostic nanomedicine. Acc Chem Res 2011; 44:1094-104; PMID:21812415; http://dx.doi.org/10.1021/ar200105p
16. Hwang SY, Cho Y, Kim HK, Cho SH, Choo J, Yoon WJ, Lee EK. Preparation of targeting proteoliposome by postinsertion of a linker molecule conjugated with recombinant human epidermal growth factor. Bioconjug Chem 2010; 21:345-51; PMID:20078100; http://dx.doi.org/10.1021/bc9004409
17. Barenholz Y. Doxil®--the first FDA-approved nano-drug: lessons learned. J Control Release 2012; 160:117-34; PMID:22484195; http://dx.doi.org/10.1016/j.jconrel.2012.03.020
18. Andreopoulou E, Gaiotti D, Kim E, Downey A, Mirchandani D, Hamilton A, Jacobs A, Curtin J, Muggia F. Pegylated liposomal doxorubicin HCL (PLD; Caelyx/Doxil): experience with long-term maintenance in responding patients with recurrent epithelial ovarian cancer. Ann Oncol 2007; 18:716-21; PMID:17301073; http://dx.doi.org/10.1093/annonc/mdl484
19. Zhang T, Chen J, Zhang Y, Shen Q, Pan W. Characterization and evaluation of nanostructured lipid carrier as a vehicle for oral delivery of etoposide. Eur J Pharm Sci 2011; 43:174-9; PMID:21530654; http://dx.doi.org/10.1016/j.ejps.2011.04.005
20. Sengupta S, Tyagi P, Velpandian T, Gupta YK, Gupta SK. Etoposide encapsulated in positively charged liposomes: pharmacokinetic studies in mice and formulation stability studies. Pharmacol Res 2000; 42:459-64; PMID:11023708; http://dx.doi.org/10.1006/phrs.2000.0714
21. Wu W, Huang J, Liu S, Li X, Cai Y. [Study on pharmacokinetics and tissue distribution of stealth matrine liposomes in rats]. Zhongguo Zhong Yao Za Zhi 2009; 34:751-5; PMID:19624022
22. Manjappa AS, Chaudhari KR, Venkataraju MP, Dantuluri P, Nanda B, Sidda C, Sawant KK, Murthy RS. Antibody derivatization and conjugation strategies: application in preparation of stealth immunoliposome to target chemotherapeutics to tumor. J Control Release 2011; 150:2-22; PMID:21095210; http://dx.doi.org/10.1016/j.jconrel.2010.11.002
23. Wong JY, Kuhl TL, Israelachvili JN, Mullah N, Zalipsky S. Direct measurement of a tethered ligand-receptor interaction potential. Science 1997; 275:820-2; PMID:9012346; http://dx.doi.org/10.1126/science.275.5301.820
24. Maruyama K, Takizawa T, Yuda T, Kennel SJ, Huang L, Iwatsuru M. Targetability of novel immunoliposomes modified with amphipathic poly(ethylene glycol)s conjugated at their distal terminals to monoclonal antibodies. Biochim Biophys Acta 1995; 1234:74-80; PMID:7880861; http://dx.doi.org/10.1016/0005-2736(94)00263-O
25. Posse de Chaves E, Sipione S. Sphingolipids and gangliosides of the nervous system in membrane function and dysfunction. FEBS Lett 2010; 584:1748-59; PMID:20006608; http://dx.doi.org/10.1016/j.febslet.2009.12.010
26. Pagnan G, Montaldo PG, Pastorino F, Raffaghello L, Kirchmeier M, Allen TM, Ponzoni M. GD2-mediated melanoma cell targeting and cytotoxicity of liposome-entrapped fenretinide. Int J Cancer 1999; 81:268-74; PMID:10188730; http://dx.doi.org/10.1002/(SICI)1097-0215(19990412)81:2<268::AID-IJC17>3.0.CO;2-1
27. Wiegandt H. The chemical constitution of gangliosides of the vertebrate nervous system. Behav Brain Res 1995; 66:85-97; PMID:7755905; http://dx.doi.org/10.1016/0166-4328(94)00129-4
28. Yu AL, Gilman AL, Ozkaynak MF, London WB, Kreissman SG, Chen HX, Smith M, Anderson B, Villablanca JG, Matthay KK, et al.; Children's Oncology Group. Anti-GD2 antibody with GM-CSF, interleukin-2, and isotretinoin for neuroblastoma. N Engl J Med 2010; 363:1324-34; PMID:20879881; http://dx.doi.org/10.1056/NEJMoa0911123
29. Czaplicki D, Horwacik I, Kowalczyk A, Wieczorek A, Bolek-Marzec K, Balwierz W, Kozik A, Rokita H. New method for quantitative analysis of GD2 ganglioside in plasma of neuroblastoma patients. Acta Biochim Pol 2009; 56:423-31; PMID:19724779
30. Cheung NK, Saarinen UM, Neely JE, Landmeier B, Donovan D, Coccia PF. Monoclonal antibodies to a glycolipid antigen on human neuroblastoma cells. Cancer Res 1985; 45:2642-9; PMID:2580625
31. Cheung NK, Dyer MA. Neuroblastoma: developmental biology, cancer genomics and immunotherapy. Nat Rev Cancer 2013; 13:397-411; PMID:23702928; http://dx.doi.org/10.1038/nrc3526
32. Munn DH, Cheung NK. Interleukin-2 enhancement of monoclonal antibody-mediated cellular cytotoxicity against human melanoma. Cancer Res 1987; 47:6600-5; PMID:3499978
33. Kushner BH, Cheung IY, Kramer K, Modak S, Cheung NK. High-dose cyclophosphamide inhibition of humoral immune response to murine monoclonal antibody 3F8 in neuroblastoma patients: broad implications for immunotherapy. Pediatr Blood Cancer 2007; 48:430-4; PMID:16421906; http://dx.doi.org/10.1002/pbc.20765
34. Loi M, Marchiò S, Becherini P, Di Paolo D, Soster M, Curnis F, Brignole C, Pagnan G, Perri P, Caffa I, et al. Combined targeting of perivascular and endothelial tumor cells enhances anti-tumor efficacy of liposomal chemotherapy in neuroblastoma. J Control Release 2010; 145:66-73; PMID:20346382; http://dx.doi.org/10.1016/j.jconrel.2010.03.015
35. Pastorino F, Brignole C, Loi M, Di Paolo D, Di Fiore A, Perri P, Pagnan G, Ponzoni M. Nanocarrier-mediated targeting of tumor and tumor vascular cells improves uptake and penetration of drugs into neuroblastoma. Front Oncol 2013; 3:190; PMID:23936762; http://dx.doi.org/10.3389/fonc.2013.00190
36. Brignole C, Pastorino F, Marimpietri D, Pagnan G, Pistorio A, Allen TM, Pistoia V, Ponzoni M. Immune cell-mediated antitumor activities of GD2-targeted liposomal c-myb antisense oligonucleotides containing CpG motifs. J Natl Cancer Inst 2004; 96:1171-80; PMID:15292389; http://dx.doi.org/10.1093/jnci/djh221
37. Gentine P, Bourel-Bonnet L, Frisch B. Modified and derived ethanol injection toward liposomes: development of the process. J Liposome Res 2013; 23:11-9; PMID:23020802; http://dx.doi.org/10.3109/08982104.2012.717298
38. Ali-Rahmani F, Hengst JA, Connor JR, Schengrund CL. Effect of HFE variants on sphingolipid expression by SH-SY5Y human neuroblastoma cells. Neurochem Res 2011; 36:1687-96; PMID:21243428; http://dx.doi.org/10.1007/s11064-011-0403-8
39. Di Paolo D, Ambrogio C, Pastorino F, Brignole C, Martinengo C, Carosio R, Loi M, Pagnan G, Emionite L, Cilli M, et al. Selective therapeutic targeting of the anaplastic lymphoma kinase with liposomal siRNA induces apoptosis and inhibits angiogenesis in neuroblastoma. Mol Ther 2011; 19:2201-12; PMID:21829174; http://dx.doi.org/10.1038/mt.2011.142
40. Macia E, Ehrlich M, Massol R, Boucrot E, Brunner C, Kirchhausen T. Dynasore, a cell-permeable inhibitor of dynamin. Dev Cell 2006; 10:839-50; PMID:16740485; http://dx.doi.org/10.1016/j.devcel.2006.04.002
41. Tivnan A, Orr WS, Gubala V, Nooney R, Williams DE, McDonagh C, Prenter S, Harvey H, Domingo-Fernández R, Bray IM, et al. Inhibition of neuroblastoma tumor growth by targeted delivery of microRNA-34a using anti-disialoganglioside GD2 coated nanoparticles. PLoS One 2012; 7:e38129; PMID:22662276; http://dx.doi.org/10.1371/journal.pone.0038129
42. Hope MJ, Bally MB, Webb G, Cullis PR. Production of large unilamellar vesicles by a rapid extrusion procedure: characterization of size distribution, trapped volume and ability to maintain a membrane potential. Biochim Biophys Acta 1985; 812:55-65; PMID:23008845; http://dx.doi.org/10.1016/0005-2736(85)90521-8
43. Krasnici S, Werner A, Eichhorn ME, Schmitt-Sody M, Pahernik SA, Sauer B, Schulze B, Teifel M, Michaelis U, Naujoks K, et al. Effect of the surface charge of liposomes on their uptake by angiogenic tumor vessels. Int J Cancer 2003; 105:561-7; PMID:12712451; http://dx.doi.org/10.1002/ijc.11108
44. Litzinger DC, Buiting AM, van Rooijen N, Huang L. Effect of liposome size on the circulation time and intraorgan distribution of amphipathic poly(ethylene glycol)-containing liposomes. Biochim Biophys Acta 1994; 1190:99-107; PMID:8110825; http://dx.doi.org/10.1016/0005-2736(94)90038-8
45. Liu D, Mori A, Huang L. Role of liposome size and RES blockade in controlling biodistribution and tumor uptake of GM1-containing liposomes. Biochim Biophys Acta 1992; 1104:95-101; PMID:1550858; http://dx.doi.org/10.1016/0005-2736(92)90136-A
46. Chang WK, Tai YJ, Chiang CH, Hu CS, Hong PD, Yeh MK. The comparison of protein-entrapped liposomes and lipoparticles: preparation, characterization, and efficacy of cellular uptake. Int J Nanomedicine 2011; 6:2403-17; PMID:22072876
47. Sheikh KA, Deerinck TJ, Ellisman MH, Griffin JW. The distribution of ganglioside-like moieties in peripheral nerves. Brain 1999; 122:449-60; PMID:10094254; http://dx.doi.org/10.1093/brain/122.3.449
48. Yu RK, Tsai YT, Ariga T. Functional roles of gangliosides in neurodevelopment: an overview of recent advances. Neurochem Res 2012; 37:1230-44; PMID:22410735; http://dx.doi.org/10.1007/s11064-012-0744-y
49. Pastorino F, Brignole C, Marimpietri D, Sapra P, Moase EH, Allen TM, Ponzoni M. Doxorubicin-loaded Fab' fragments of anti-disialoganglioside immunoliposomes selectively inhibit the growth and dissemination of human neuroblastoma in nude mice. Cancer Res 2003; 63:86-92; PMID:12517782
50. Cheung NK, Guo H, Hu J, Tassev DV, Cheung IY. Humanizing murine IgG3 anti-GD2 antibody m3F8 substantially improves antibody-dependent cell-mediated cytotoxicity while retaining targeting in vivo. Oncoimmunology 2012; 1:477-86; PMID:22754766; http://dx.doi.org/10.4161/onci.19864
51. Licciardi M, Paolino D, Celia C, Giammona G, Cavallaro G, Fresta M. Folate-targeted supramolecular vesicular aggregates based on polyaspartylhydrazide copolymers for the selective delivery of antitumoral drugs. Biomaterials 2010; 31:7340-54; PMID:20609469; http://dx.doi.org/10.1016/j.biomaterials.2010.05.060